

Thermodynamic Assessment of Slag–Matte–Metal Equilibria in the Cu–Fe–O–S–Si System

Denis Shishin¹ · Evgueni Jak¹ · Sergei A. Decterov^{1,2}

Submitted: 1 May 2018 / in revised form: 29 June 2018 / Published online: 13 August 2018
© ASM International 2018

Abstract Equilibria among the slag, matte and metal phases in the Cu–Fe–O–S–Si system are critically assessed using thermodynamic modeling. The relationships among matte grade, temperature, partial pressure of SO₂, Fe/SiO₂ in the slag, and the copper concentration in the slag are described by the model, as well as the concentrations of other elements in all phases. A thermodynamic database is created, which can be used for understanding and improving the pyrometallurgical production of copper. An extensive experimental dataset includes the most recent results obtained by the equilibration/quenching/EPMA analysis technique. These data allow to distinguish the physical entrainment of the matte and solid phases in the slag from chemical solubility. As a result, it is possible to describe the copper solubility in the slag with high accuracy and establish the relationship between copper and sulfur in the slag. The thermodynamic database of the present study is consistent with previously reported thermodynamic evaluations of binary, ternary and quaternary subsystems. The slag phase is modeled using the two-sublattice modified quasichemical model in the quadruplet

approximation. The matte and metal liquid phases are modeled as one solution using the single-sublattice modified quasichemical model in the pair approximation.

Keywords CALPHAD approach · critical assessment · liquidus · optimization · phase diagram · thermodynamic properties · thermodynamic modeling

1 Introduction

Cu–Fe–O–S–Si is the basic chemical system for copper and mixed lead–copper smelting. Thermodynamic modeling of the Cu–Fe–O–S–Si system was conducted by Decterov and Pelton.^[1] The resulting thermodynamic database predicted phase equilibria between solids and liquids, solubilities and activities of components in these phases, as well as heat balance. The authors attributed a portion of copper and sulfur concentrations in the slag reported in some studies to the physically entrained matte. Therefore, the model predicted relatively low copper solubility in the slag. Oxygen solubility in the matte was not taken into account. Only limited data close to tridymite saturation were available at the time, so that the effect of the Fe/SiO₂ ratio in the slag was not analyzed. The results were combined with the extensive oxide database^[2–4] and included into the FactSage software package,^[5] version 5.6 and later.

Recent experimental studies by Chen et al.,^[6,7] Hidayat et al.^[8–11] and Fallah-Mehrjardi et al.^[12–16] provide a quantitative description of the effect of the Fe/SiO₂ ratio, temperature and $P(\text{SO}_2)$ on all phase constituents. A combination of the substrate technique, gas flow equilibration, ultra-rapid quenching and electron probe microanalysis (EPMA) allowed distinguishing between the chemical solubilities and entrainment. Substrate technique implies that a

This invited article is part of a special issue of the *Journal of Phase Equilibria and Diffusion* in honor of Prof. Zhanpeng Jin's 80th birthday. The special issue was organized by Prof. Ji-Cheng (JC) Zhao, The Ohio State University; Dr. Qing Chen, Thermo-Calc Software AB; and Prof. Yong Du, Central South University.

✉ Sergei A. Decterov
Sergei.Decterov@polymtl.ca

¹ PYROSEARCH, The University of Queensland, Brisbane, Australia

² Dép. de Génie Chimique, École Polytechnique, Centre de Recherche en Calcul Thermochimique (CRCT), Montreal, QC, Canada

saturation phase acts as a holding vessel for slag and matte, preventing the contamination by the crucible material.^[9] These experimental studies are part of the project currently under way at the PYROSEARCH (Pyrometallurgy Innovation Center). The aim is to develop a thermodynamic database for the Al-Ca-Cu-Fe-Mg-Si-O-Pb-S-Zn multi-component chemical system, including also minor components As, Bi, Sb, Sn, Ag, and Au, which will be particularly useful for pyrometallurgical applications.^[17]

The present article reports a thermodynamic assessment of the Cu-Fe-O-S-Si system, taking into account the new experimental data. All relevant thermodynamic and phase diagram data are critically evaluated. Model parameters for the Gibbs energies of all phases as functions of temperature and composition are optimized simultaneously based on the assessed data. From these equations, all of the thermodynamic properties and phase diagrams can be back-calculated and compared with the experimental data. In this way, all the data are rendered self-consistent and consistent with thermodynamic principles. Thermodynamic property data, such as enthalpies and activities, aid in the evaluation of phase diagrams and vice versa. The results of thermodynamic optimizations for the binary, ternary and quaternary subsystems were published earlier: Fe-O,^[18] Cu-S, Fe-S, Cu-Fe-S,^[19–21] Cu-O and Cu-O-S,^[22] Cu-Fe-O,^[23] Fe-O-S,^[24] Cu-Fe-O-S,^[25] Cu-O-Si,^[26] Fe-O-Si^[27] and Cu-Fe-O-Si.^[28] The limited experimental data on the Fe-O-S-Si quaternary system are evaluated in the present study. Thermodynamic calculations are performed using the FactSage software package.^[29]

2 Thermodynamic Models

The list of stable phases in the Cu-Fe-O-S-Si system is given in Table 1. The thermodynamic assessments of several subsystems and the corresponding optimized model parameters were reported earlier.^[24,30–40] The phases underlined in Table 1 are the focus of the present study.

The liquid phases observed in the pyrometallurgical production of copper are slag (oxide liquid), matte (sulfide liquid) and liquid copper (metallic liquid). These three liquids may be regarded as one complex solution with miscibility gaps. In fact, the metallic and oxide liquids in the Cu-O subsystem are completely soluble above 1350 °C.^[22] There is no miscibility gap between the metal and matte in the Fe-S subsystem.^[19] The oxysulfide liquid phase in the Fe-O-S subsystem expands from molten nonstoichiometric FeS all the way towards FeO-Fe₂O₃ liquid.^[24] It is the addition of SiO₂ to the Fe-O-S system that causes the appearance of the miscibility gap between the SiO₂-containing slag phase and the S-rich matte phase.^[41]

In principle, it is possible to describe the oxide, sulfide and metallic liquids as one solution with miscibility gaps.

Dilner and Selleby^[42] used the ionic two-sublattice liquid model $(Ca^{+2}, Fe^{+2})_p(O^{-2}, S^{-2}, Vacancy^{-Q}, FeO_{1.5}, S_0)_Q$ to describe the slag, matte and metal liquids in the assessment of the Ca-Fe-O-S system. The major features of the system were successfully reproduced by the model, but some systematic deviations from the experimental data were observed in the S/(O + S) molar ratios of the oxide-rich and sulfide-rich liquids in equilibrium. The extension of this oxysulfide model to SiO₂-containing systems has not been reported yet.

The modified quasichemical model in the pair approximation (MQMPA) was used by the present authors to describe the oxide, sulfide and metallic liquids as a single solution in the Cu-Fe-O-S system.^[25] It takes into account the first-nearest-neighbor short-range ordering (FNN SRO) between metals and non-metals. However, if Si is added to the system, the second-nearest-neighbor short-range ordering (SNN SRO) between Fe²⁺ and Si⁴⁺ cations becomes important. It is not possible to take this into account explicitly within the scope of the MQMPA.

Jo et al.^[43] used the modified quasichemical model in the quadruplet approximation (MQMQA) to describe the oxysulfide liquid $(Mn^{2+}, Fe^{2+}, Si^{4+})(O^{2-}, S^{2-})$. Since it was intended for the use in the steel industry at low $P(O_2)$, the presence of Fe³⁺ ions was neglected. This model also does not take into account the deviation of the liquid composition from stoichiometric oxides and sulfides, which becomes particularly important for the sulfur-rich liquid that can expand to the pure liquid metal. The model described the appearance and expansion of the slag-matte miscibility gap with the addition of SiO₂ to FeO-FeS oxysulfide. Since this model does not allow the deviation of the stoichiometry towards metal, the metallic liquid was represented by a separate solution.

A solution model describing simultaneously slag, matte and liquid metal should take into account at least the major interactions in the liquid phase, which are the FNN SRO between cations and anions, the deviation of the stoichiometry towards metal, and the SNN SRO between acidic and basic oxides. In principle, it is possible to develop such a model using the two-sublattice modified quasichemical formalism in the quadruplet approximation, but it will be very difficult to properly calibrate such a model, because the experimental information for the composition regions where the nature of the liquid changes from oxide to sulfide to liquid metal is scarce. Essentially, many model parameters would not be constrained by experimental data and would have to be gestimated, which could adversely affect the predictive ability of the model even in the predominantly oxide, sulfide and metal regions.

Table 1 List of oxide, sulfide, metallic and sulfate phases in the Cu-Fe-O-S-Si system at ambient total pressure

Phase name	Model, reference for parameters	Short notation
<i>Oxide phases</i>		
Cuprous, cupric oxides	Stoichiometric compounds ^[22]	Cu ₂ O, CuO
Quartz/tridymite/cristobalite	Stoichiometric compound ^[70]	Qz/trid/crist (SiO ₂)
Delafossite	Stoichiometric compound ^[23,28]	CuFeO ₂
Fayalite	Stoichiometric compound ^[27]	Fe ₂ SiO ₄
Hematite	Stoichiometric compound ^[18]	Fe ₂ O ₃
Spinel (magnetite)	(Cu ²⁺ , Fe ²⁺ , Fe ³⁺) ^{etr} [Cu ²⁺ , Fe ²⁺ , Fe ³⁺ , Va] ₂ ^{oct} O ₄ ²⁻ , CEF ^[18,23]	Spinel
Monoxide (Wüstite)	(FeO, FeO _{1.5} , CuO), BW ^[18,23]	Wüstite
Liquid oxide (slag)	(Cu ¹⁺ , Fe ²⁺ , Fe ³⁺ , Si ⁴⁺)(O ²⁻ , S ²⁻), MQMQA ^[26–28]	Slag
<i>Sulfide phases</i>		
Liquid matte/metal	(Fe ^{II} , Fe ^{III} , Cu ^I , Cu ^{II} , O ^{II} , S ^{II}), MQMPA ^[18–25]	Matte, liq metal
Pyrrhotite	(Fe, Cu, vacancy)S, BW ^[19,21]	
Digenite-bornite	(Cu ₂ , Fe, vacancy)S, BW ^[20]	
Intermediate solid sulfide solution	(Cu ₂ , Fe, vacancy)S, BW ^[20]	
<i>Metallic phases</i>		
fcc-Cu and fcc-Fe	(Fe, Cu, O, S), BW ^[18,22,23]	Cu(fcc)/Fe(fcc)
bcc-Fe	(Fe, Cu, O, S), BW ^[18]	Fe(bcc)
<i>Sulfate phases</i>		
FeSO ₄ , Fe ₂ (SO ₄) ₃ , CuSO ₄ , Cu ₂ SO ₄ , CuO-CuSO ₄	Stoichiometric compounds ^[22,24,25]	

References are given for thermodynamic model parameters

BW Bragg–Williams model, CEF compound energy formalism, MQMQA modified quasichemical model in the quadruplet approximation, MQMPA modified quasichemical model in the pair approximation

Hence, a more practical approach was adopted in the present study, i.e. the matte and metallic liquid were described as a single solution using the MQMPA, while the slag is modeled using the MQMQA as a separate solution. This choice is based on the fact that under the conditions relevant to pyrometallurgy, the deviations of the slag stoichiometry towards metal are negligible, while both FNN SRO and SNN SRO are important and must be explicitly taken into account, which can be done by the two-sublattice MQMQA. Furthermore, the slag solution optimized in the present study for the Cu-Fe-O-S-Si system must be compatible with the much larger oxide database developed earlier, which uses the MQMQA for the liquid phase. On the other hand, under the conditions of copper production, the solubility of Si in the matte and metal is extremely low and can be neglected, so that the SNN SRO is not important for those liquids. Hence, the MQMPA is sufficient to describe the most important interactions in both sulfide and metallic liquids. The model for the matte/metal phase was adopted from previous publications^[18–25] without modifications. The benefits and limitations of this approach are demonstrated throughout the paper.

2.1 Slag

Liquid oxide (slag) is an ionic melt, which is reflected in the model by placing cations and anions on separate sublattices as shown in Table 1. The Gibbs energy expression is given by^[44]:

$$G = \sum_{\substack{ij \\ k,l}} n_{ij/kl} g_{ij/kl} - T \Delta S^{\text{config}} \quad (\text{Eq 1})$$

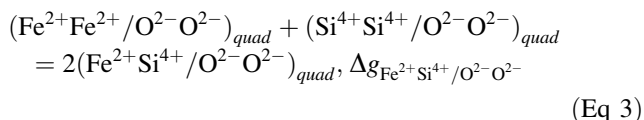
where $i, j = \text{Cu}^{1+}, \text{Fe}^{2+}, \text{Fe}^{3+}, \text{Si}^{4+}$ and $k, l = \text{O}^{2-}, \text{S}^{2-}$, $n_{ij/kl}$ and $g_{ij/kl}$ are the number of moles and the molar Gibbs energy of the ij/kl quadruplet, ΔS^{config} is the configuration entropy of mixing. For the concept of quadruplets and discussion of the distinction between quadruplets and associates or molecules the reader is referred to the publication by Pelton et al.^[44] An application of the MQMQA formalism to oxysulfide liquid was reported by Piao et al.^[45]

The Gibbs energies of unary quadruplets, ii/kk , are obtained from the Gibbs energies of pure oxides and sulfides. For example:

$$g_{\text{Fe}^{2+}\text{Fe}^{2+}/\text{O}^{2-}\text{O}^{2-}} = \left(\frac{2}{Z_{\text{Fe}^{2+}\text{Fe}^{2+}/\text{O}^{2-}\text{O}^{2-}}} \right) g_{\text{FeO}}^{\circ} \quad (\text{Eq 2})$$

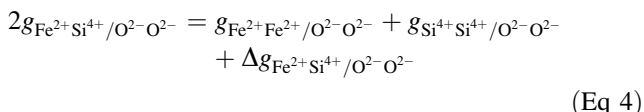
where $Z_{ij/kl}^i$ is the SNN coordination number of i species when (hypothetically) all i species exist in the ij/kl quadruplet, and g_{FeO}° is the standard molar Gibbs energy of pure liquid FeO. The magnitude of the Gibbs energies of the unary quadruplets determine the level of FNN SRO between cations and anions.

The formation of the second-nearest-neighbor (Fe^{2+} - $[\text{O}^{2-}]\text{-Si}^{4+}$) pairs in the FeO-SiO₂ system can be written as the following reaction between quadruplets:



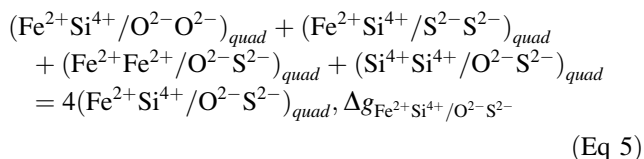
where the Gibbs energy of this reaction, $\Delta g_{\text{Fe}^{2+}\text{Si}^{4+}/\text{O}^{2-}\text{O}^{2-}}$, is a model parameter, which determines the degree of SNN SRO. It can be further expanded as a polynomial as discussed in more detail by Pelton et al.^[44]

Hence, the Gibbs energies for the binary quadruplets ij/kl are obtained as follows:

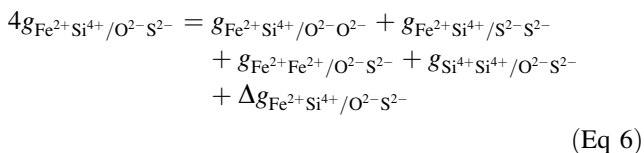


Similar equations are used for the binary quadruplets of the ii/kl type.

Finally, the reciprocal quadruplet may be obtained by the reaction



so that the Gibbs energy of the reciprocal quadruplet can be estimated from the Gibbs energy of this reaction and the Gibbs energies of the binary quadruplets:



ΔS^{config} is given by randomly distributing all the quadruplets over “quadruplet positions”, taking into the account the fact that anion-cation pairs are shared among quadruplets. Because an exact mathematical expression for such distribution is not known, an approximate equation was proposed.^[44] A slightly modified version of this equation is used in the present study, which can be found in appendix 1 of the Ph.D. thesis of Lambotte.^[30]

The equilibrium amounts of different quadruplets are obtained by minimizing the Gibbs energy given by Eq 1.

3 Assessment of the Experimental Data for the Slag–Matte Equilibrium

The thermodynamic equilibria between the slag and matte in the Cu-Fe-O-S-Si system were studied by Yazawa and Kameda,^[31] Kameda and Yazawa,^[32] Korakas,^[33] Kuxmann and Bor,^[34] Bor and Tarassoff,^[35] Geveci and Rosenqvist,^[36] Nagamori,^[37] Tavera and Davenport,^[38] Kaiura et al.,^[39] Jalkanen,^[46] Yazawa et al.,^[47] Shimpo et al.,^[48] Tavera and Bedolla,^[49] Li and Rankin,^[50] Takeda,^[40,51] Font et al.^[52] New data were reported recently by Chen et al.,^[6,7] Hidayat et al.^[8–11] and Fallah-Mehrjardi et al.^[12–14]

According to the Gibbs phase rule applied to the Cu-Fe-O-S-Si system, the number of degrees of freedom $F = 5 + 2 - n$, where n is the number of phases in thermodynamic equilibrium. The following degrees of freedom are normally fixed when the system is studied experimentally. (1) Temperature, which is usually selected in the range from 1200 to 1300 °C and kept constant. (2) Total pressure of 1 atm. (3) Presence of the slag phase. (4) Presence of the matte phase. (5) Fixed Fe/SiO₂ ratio in the slag, which is usually achieved either by tridymite saturation, giving the lowest possible Fe/SiO₂, or by spinel saturation, corresponding to the highest Fe/SiO₂. Intermediate Fe/SiO₂ values are hard to keep fixed during the experiment. The sample should be kept in a crucible, which is usually made of SiO₂. Crucibles made from MgO, Al₂O₃ or other materials result in contamination of the slag or matte phase. Using the Fe₃O₄ spinel substrate as a holding material is a novel technique developed by PYROSEARCH.^[9] (6) Fixed partial pressure of SO₂. This can be done by controlling the gas flow in an open-crucible setup. Another option is to introduce the metal phase in a closed-crucible setup, which corresponds to the lowest possible $P(\text{SO}_2)$. The metal phase is either solid Fe, or liquid Cu-Fe alloy. The low- $P(\text{SO}_2)$ conditions in equilibrium with the metal phase are far from those observed in the industry, but were preferred by the authors of the earlier experimental studies due to a relatively simple experimental setup. (7) The last degree of freedom can be set by changing the Cu₂S/FeS ratio in the initial mixture, or by varying $P(\text{O}_2)$ in the controlled gas flow. If all degrees of freedom are properly fixed, the slag and matte in equilibrium will have a certain, or invariant, composition. In practice, a series of experiments is usually performed by fixing all degrees of freedom except one, which is varied. The results can then be presented as lines on two-dimensional plots. The widely accepted X-axis for these plots is the wt.% of Cu in the matte, which is often referred to as the matte grade. Even though it is not fixed directly in the experiment and changes as a result of equilibration,

following the variation of the selected degree of freedom, it can be measured with high accuracy after the experiment. Sometimes the wt.% of Fe in the matte or $P(\text{O}_2)$ are used as the X-axis.

An example of a proper experimental setup is the study of Hidayat et al.^[9] The temperature was set at 1200 °C (1); an open crucible setup gives the total pressure of 1 atm. (2); the presence of the slag (3) and matte (4) phases was verified by SEM after the experiment; the sample was kept on a spinel substrate and an equilibrium with spinel (5) was confirmed by measuring the copper content in quenched spinel crystals using EPMA; and the last two degrees of freedom were fixed by equilibrating the sample with the flow of CO-CO₂-SO₂-Ar gas mixtures, which defined $P(\text{SO}_2)$ and $P(\text{O}_2)$. The composition of the gas was calculated to keep $P(\text{SO}_2)$ constant at 0.25 atm., while $P(\text{O}_2)$ was increased stepwise to produce approximately equal gains in wt.% Cu in the matte phase. These experiments required advanced planning. A preliminary thermodynamic database was used to predict the starting compositions. The measured compositions of equilibrated phases were presented as functions of the Cu/(Cu + Fe + S) mass ratio in the matte, which was reliably measured by EPMA after the experiment.

An example of the experimental setup violating the Gibbs phase rule is the study by Tavera and Bedolla.^[49] The temperature was fixed at 1200 or 1300 °C (1); total pressure was 1 atm. (2); the slag (3) and matte (4) phases were present; the experiments were conducted in silica crucibles (5); metallic copper (6) was an additional phase obtained in the experiments; a flow of CO-CO₂-SO₂-Ar gas was passed through the system, thus imposing 2 more degrees of freedom: $P(\text{SO}_2)$ (7) and $P(\text{O}_2)$ (8). As a result, the system was “overfixed”, which manifested itself in the fact that the measured O and S contents of the metallic copper were significantly different from equilibrium amounts reported by other authors.

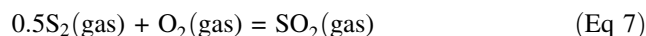
The following Sect. 3.1-3.3 summarize the experimental data on the slag–matte equilibria and analyze the consistency between them. The observed trends are explained. Model predictions are used when experimental data are unavailable or inconclusive. The optimization of model parameters and discussion of the agreement between the obtained thermodynamic database and experimental data are presented in Sect. 4.

3.1 Slag–Matte Equilibrium: General Trends and Effect of Temperature

Figure 1 combines the data for the slag–matte equilibrium at silica saturation and relatively high fixed $P(\text{SO}_2)$ to demonstrate general trends and the effect of temperature.

Each specific line or symbol corresponds to the same equilibrium throughout Fig. 1.

The general trends observed in Fig. 1 can be understood based on the fact that binary Fe-O pair interactions are stronger than Cu-O and Fe-S interactions. Hence, if the matte and slag are equilibrated at certain temperature and oxygen partial pressure and then $P(\text{O}_2)$ is increased, iron will be oxidized from the matte into slag forming more Fe-O FNN pairs and the matte grade will increase. This reaction is also aided by the strong SNN interactions between Fe²⁺ and Si⁴⁺ cations in the slag, i.e. iron is fluxed by silica into the slag phase. Hence, the equilibrium oxygen partial pressure increases monotonically with matte grade (Fig. 1a). Partial pressure of sulfur decreases (Fig. 1b), which is due to the equilibrium reaction at fixed $P(\text{SO}_2)$:



Naturally, iron in the matte decreases with matte grade (Fig. 1c). Since the Fe-O pair interactions in the matte phase are stronger than the interactions with oxygen of all other matte components, oxygen is present in the matte mostly in the Fe-O FNN pairs. Because of this, the oxygen content in the matte diminishes when the iron content goes down (Fig. 1d) until there is almost no iron left in the matte and the equilibrium $P(\text{O}_2)$ becomes high enough to allow some Cu-O pairs to form, which explains the slight increase in the oxygen content at about 80 wt.% Cu in the matte.

Sulfur in the matte goes through a maximum (Fig. 1e). Pure FeS contains 36 wt.% S while pure Cu₂S only 20 wt.% S. However, as the amount of copper in the matte phase decreases, the strong Fe-O pair interactions result in the replacement of the Fe-S FNN pairs by the Fe-O ones, increasing of the oxygen content at the expense of the wt.% S.

The sulfur content in the slag decreases with matte grade (Fig. 1i) due to the decrease in $P(\text{S}_2)$. Since the Fe-S pair interactions are much stronger than the Si-S ones, less silica dissolves in the slag at SiO₂ saturation and low matte grades. Furthermore, the SNN interactions (Fe²⁺-[S²⁻]-Si⁴⁺) are weaker than (Fe²⁺-[O²⁻]-Si⁴⁺), which also suppresses the solubility of SiO₂ at higher sulfur concentrations. Hence, increasing matte grade brings down the iron content in the slag expressed either as the Fe/SiO₂ ratio (Fig. 1g), or as wt.% of “FeO” (Fig. 1h). The latter is calculated assuming that Fe is present in the slag only as FeO, i.e. it equals the measured wt.% Fe multiplied by (55.845 + 15.9994)/55.845. The notation “FeO” is an oversimplification, because it ignores the presence of Fe³⁺ and the existence of the Fe²⁺-S²⁻ pairs in the slag, but it is widely used in experimental articles to represent the total iron content in slags. The amount of Fe³⁺ in the slag can be seen from the Fe³⁺/(Fe²⁺ + Fe³⁺) ratio shown in Fig. 1(f).

Fig. 1 Slag–matte equilibrium in the Cu–Fe–O–S–Si system at fixed temperature, total pressure of 1 atm., tridymite (SiO₂) saturation and fixed P(SO₂). Symbols are experimental data, [33,38–40,51,52] lines are calculated using the models of the present study. Different lines show the effect of temperature

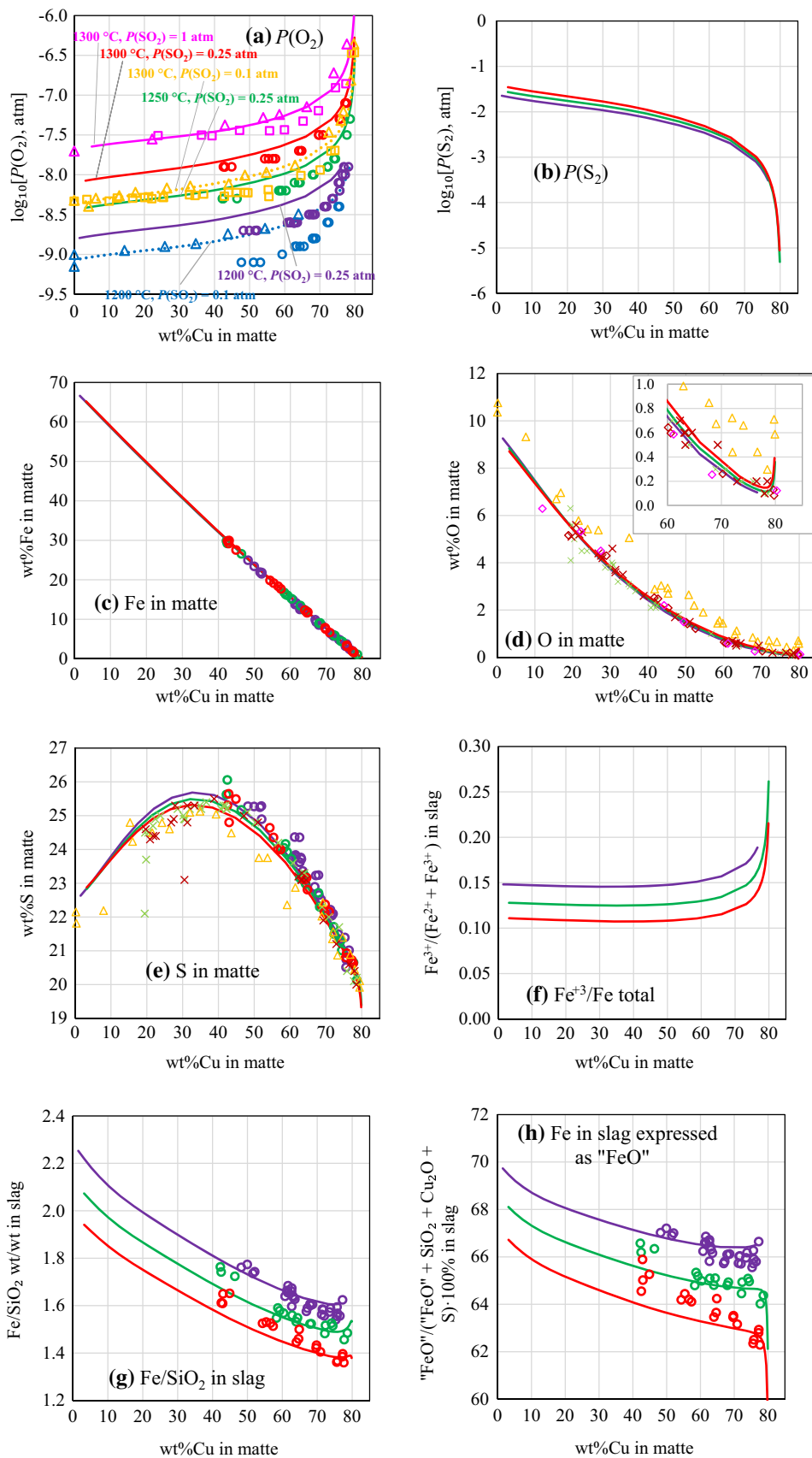
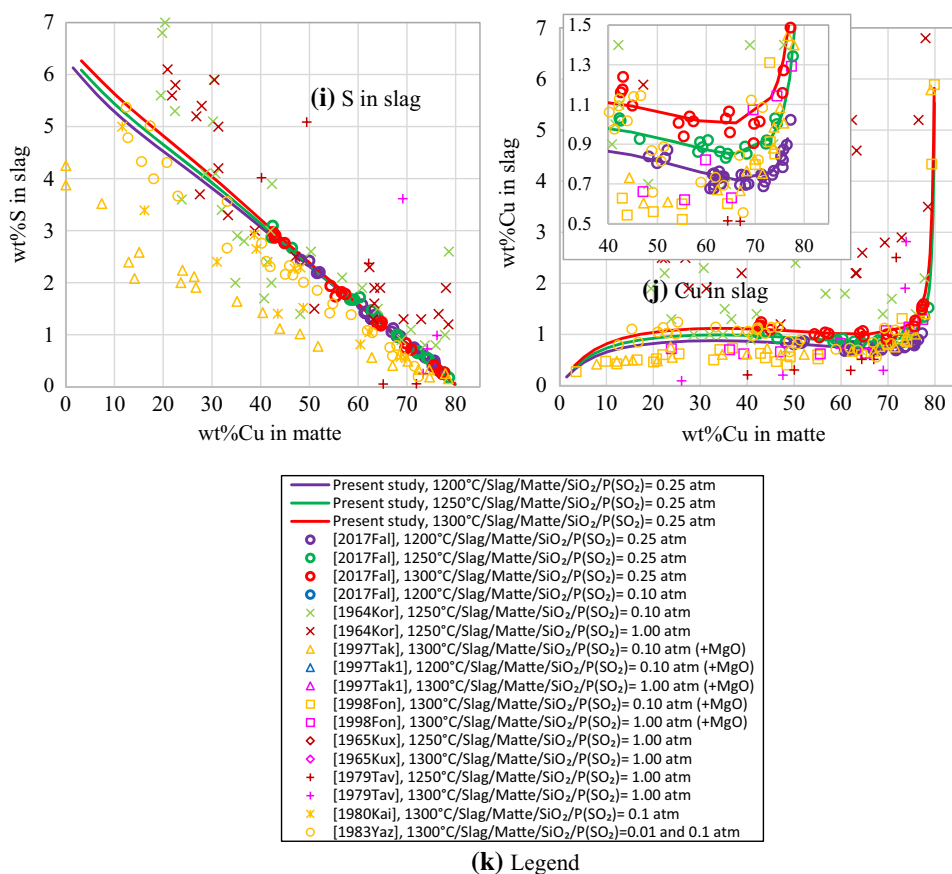


Fig. 1 continued



It was not measured experimentally under these conditions, but the calculated lines are based on the experimental data in the Cu-Fe-O-Si system.^[28] It should be noted that the iron content in Fig. 1(h) drops when approaching 80 wt.% Cu in the matte due to the dissolution of large amounts of Cu₂O in the slag. However, at 1200 °C and $P(\text{SO}_2) = 0.25$ atm. this is not realized because the calculated line terminates at spinel saturation. As can be seen from Fig. 1(g) and (h), the iron content in the slag decreases with temperature as more silica dissolves in the slag at SiO₂ saturation, which is to be expected.

The copper content in the slag goes through a maximum (Fig. 1j) at intermediate matte grades, then falls slightly and rises sharply approaching 80 wt.% Cu in the matte. The increase in equilibrium $P(\text{O}_2)$ with matte grade (Fig. 1a) should favor oxidation of copper into the slag, but this effect is counteracted by the simultaneous decrease in the sulfur content (Fig. 1i). As will be shown in Sect. 4, the exchange reaction among pure liquid oxides and sulfides, $\text{Cu}_2\text{O} + \text{FeS} = \text{Cu}_2\text{S} + \text{FeO}$, is characterized by a very negative Gibbs energy, which results in strong FNN cation–anion short-range ordering, i.e. the Fe-O and Cu-S pairs in the slag predominate at the expense of the Fe-S and Cu-O pairs. Hence, the solubility of sulfur in the slag is beneficial for the solubility of copper. The balance of the

increasing $P(\text{O}_2)$ and decreasing sulfur content accounts for the local maximum in the copper content at intermediate matte grades.

The calculated lines predict small variations in the matte composition with temperature, i.e. the decreasing S (Fig. 1e) and increasing O content (Fig. 1d). These trends can be neither confirmed nor ruled out by the experiments due to the experimental scatter.

There are a few inconsistencies in the experimental data on the slag–matte equilibria at silica saturation and fixed $P(\text{SO}_2)$.

Takeda^[40,51] measured $P(\text{O}_2)$ in situ, using an immersed oxygen sensor (Fig. 1a, triangles). ZrO₂-doped MgO was used as a solid electrolyte and the reference electrode was Ni/NiO. The gas flow mixture of Ar-SO₂-S₂ was passed over the sample. $P(\text{S}_2)$ was varied by the temperature of the sulfur bath. Takeda reported that it was difficult to completely equilibrate the gas flow with condensed phases and that the equilibrium oxygen and sulfur potentials in the matte and slag were substantially different from those in the gas phase. Hence, he measured $P(\text{O}_2)$ by immersing the oxygen sensor into the melt and calculated $P(\text{S}_2)$ from the equilibrium constant of reaction (7).

Font et al.^[52] prepared the gas mixture of Ar-SO₂-S₂ similar to Takeda^[40,51] and assumed complete equilibration

between the gas and condensed phases. $P(\text{O}_2)$ was not measured, but rather calculated from $P(\text{SO}_2)$, $P(\text{S}_2)$ and the equilibrium constant of reaction (7). The experimental points by Font et al.^[52] (Fig. 1a, squares) show systematically lower $P(\text{O}_2)$ for a given matte grade, temperature and $P(\text{SO}_2)$, with the difference up to 0.2 in $\log_{10}[P(\text{O}_2)]$.

Fallah-Mehrjardi et al.^[15] (Fig. 1a, circles) reported lower $P(\text{O}_2)$ versus matte grade at 1200 °C and $P(\text{SO}_2) = 0.1$ atm. compared to Takeda.^[40,51] The difference is up to 0.25 in $\log_{10}[P(\text{O}_2)]$. In these experiments, $P(\text{O}_2)$ was not measured, but calculated from the composition of the $\text{CO-CO}_2\text{-SO}_2\text{-Ar}$ gas flow using the thermodynamic properties of gaseous species and assuming complete equilibration between the gas and condensed phases. The latter assumption is discussed in more detail by Fallah-Mehrjardi et al.^[14] The results of the same authors at $P(\text{SO}_2) = 0.25$ ^[12] cannot be directly compared to Takeda^[40,51] and Font et al.,^[52] who reported the data only at $P(\text{SO}_2) = 0.1$ and 1 atm. However, an indirect comparison using model-predicted lines indicate that these data are also systematically lower than suggested by interpolation of the results of Takeda.^[40,51]

The experiments of Takeda^[40,51] and Font et al.^[52] were carried out in MgO crucibles, which resulted in the slags containing 6–8 and 6 wt.% MgO, respectively. However, Fallah-Mehrjardi et al.^[16] reported very small effect of MgO on the $P(\text{O}_2)$ versus matte grade curves. Hence, contamination of the slags by MgO cannot explain the difference of 0.10–0.25 in $\log_{10}[P(\text{O}_2)]$ among different studies. The calculated lines in Fig. 1(a) are mostly based on the previous assessments of the subsystems of the Cu-Fe-O-S-Si system^[18–28] and are not significantly affected by the model parameters optimized in the present study. These lines are in good agreement with the data of Takeda.^[40,51] More experimental work is needed to resolve the remaining uncertainty in equilibrium $P(\text{O}_2)$.

A systematic difference between various data sets is observed in Fig. 1(i) and (j). The copper and sulfur content of the slag measured by Takeda^[40,51] and copper content by Font et al.^[52] are lower than the results of Fallah-Mehrjardi et al.^[12–15] The slags of the former studies were contaminated by MgO from the crucible material. This resulted in the decrease of both Cu and S content in the slag for a given matte grade and the maximum on the copper solubility curve is less prominent. These data will be assessed together with other studies in a future publication on the effect of Al_2O_3 , CaO and MgO on the slag–matte equilibrium. The S content in the slag reported by Yazawa et al.^[47] is slightly lower, but the copper content is in agreement with Fallah-Mehrjardi et al.^[12–15] within the scatter of the experimental data. The results of Fallah-Mehrjardi et al.^[12–15] are accepted in the present study because superior measurement techniques were employed.

It should be noted that very high copper and sulfur contents in the slag reported by Korakas^[33] are most likely the result of physical entrainment of the matte particles in the slag.

For the oxygen content in the matte phase (Fig. 1d), the lower values of Korakas^[33] (Fig. 1d, crosses) and of Kuxmann and Bor^[34] (Fig. 1d, diamonds) were selected over Takeda's data^[40,51] (Fig. 1d, triangles). The reason is that the data of Korakas^[33] on sulfur in the matte (Fig. 1e, crosses) are in agreement with the results of Fallah-Mehrjardi et al.^[12–15] (Fig. 1e, circles).

3.2 Slag–Matte and Slag–Matte–Metal Equilibria: Effect of $P(\text{SO}_2)$

Figure 2 combines the data for the slag–matte equilibrium at silica saturation to demonstrate the effect of $P(\text{SO}_2)$. Each specific line or symbol corresponds to the same equilibrium throughout Fig. 2. The order of the diagrams is the same as in Fig. 1, but one more plot is added to show $P(\text{SO}_2)$ (Fig. 2c).

The lowest possible $P(\text{SO}_2)$, at which the slag and matte can co-exist, corresponds to the formation of a metallic phase, that is either solid iron at low matte grades or liquid Cu-Fe alloy at high matte grades (Fig. 2c). With the decrease of $P(\text{SO}_2)$, both $P(\text{O}_2)$ and $P(\text{S}_2)$ fall (Fig. 2a, b); the oxygen content in the matte decreases and reaches its lowest values at metal saturation due to the decrease in $P(\text{O}_2)$ (Fig. 2e); the sulfur content of the matte decreases at most matte grades because of the decline in $P(\text{S}_2)$, but at small matte grades this trend is reversed due to the increasing oxygen solubility in the matte (see Fig. 1e, 2f). The iron content in the slag goes down as $P(\text{SO}_2)$ decreases (Fig. 2h, i) and can be a good indicator of the effective $P(\text{SO}_2)$ in the system, since it is possible to see the difference not only between metal saturation and high $P(\text{SO}_2)$, but even between $P(\text{SO}_2) = 0.6, 0.25$ and 0.1 atm. The sulfur, copper and Fe^{3+} contents of the slag also diminish with decreasing $P(\text{SO}_2)$, reaching the lowest values at metal saturation (Fig. 2j, k, g).

Some uncertainty is observed in Fig. 2(d) and (f) for the S and Fe contents of the matte at metal saturation. Chen et al.^[6] suggested approximately the same values at metal saturation, as at high $P(\text{SO}_2)$ (Fig. 2d, f, circles). Yazawa and Kameda^[31] reported that the mattes obtained by melting Cu_2S , FeS and FeO in silica crucibles under a flow of purified nitrogen contained less sulfur and more iron (Fig. 2d, f, crosses). Similar results were later reported by Kameda and Yazawa^[32] for the mattes synthesized by melting Cu_2S , FeS and FeO in iron crucibles under flowing nitrogen (Fig. 2f, minus signs). Neither of these two studies by Yazawa and Kameda correspond to the slag–matte– SiO_2 equilibrium at fixed $P(\text{SO}_2)$ or at metal saturation. One degree of freedom remained unfixed in both cases, so that the composition of the

Fig. 2 Slag–matte equilibria in the Cu-Fe-O-S-Si system at fixed temperature, total pressure of 1 atm., tridymite (SiO_2) saturation and at fixed $P(\text{SO}_2)$ or in equilibrium with metal, which is solid Fe or liquid Cu-Fe alloy. Symbols are experimental data, [6,7,15,31,32,35,48,49,51,54] lines are calculated using the models of the present study. Different lines show the effect of $P(\text{SO}_2)$

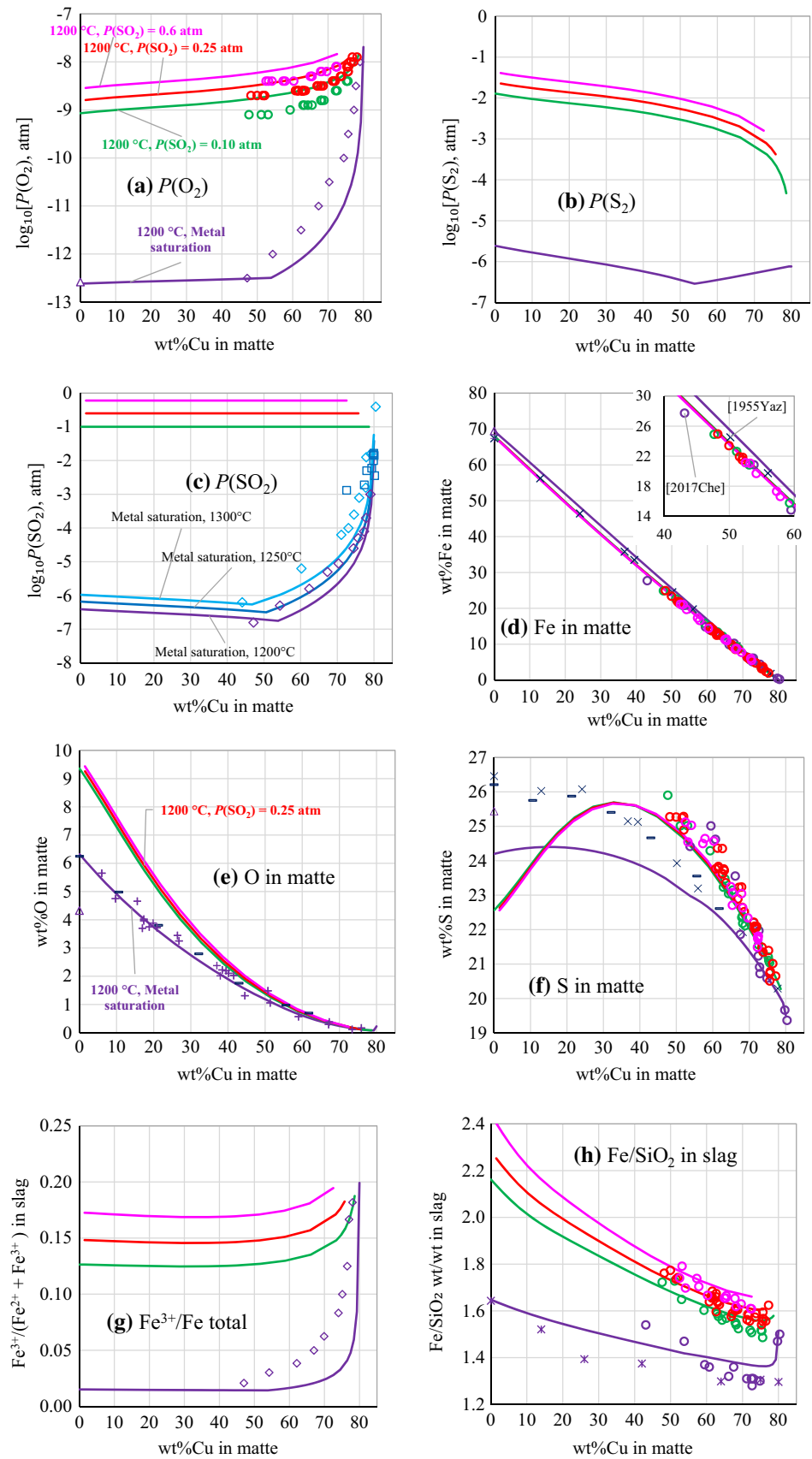
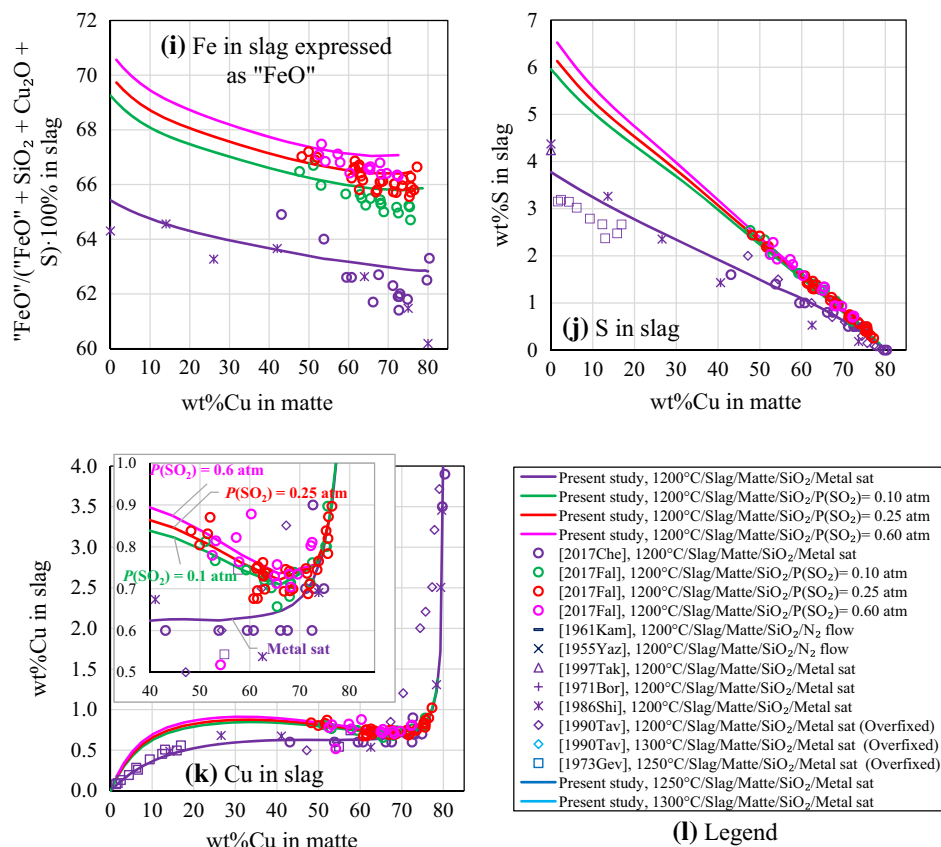


Fig. 2 continued



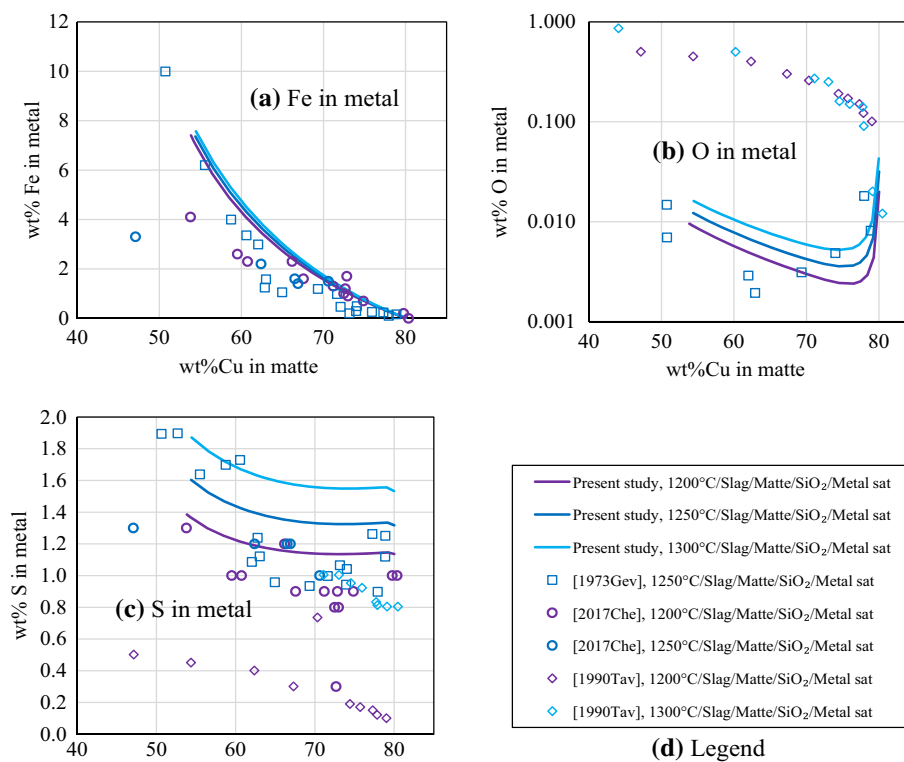
mattes was essentially determined by the amounts of the initial reactants. Hence, the synthesized mattes remained very close to the oxysulfide Cu₂S-FeS-FeO plain with no deviation towards metal. This was assumed in the former study,^[31] in which the mattes were analyzed only for Cu, Fe and S, and confirmed later^[32] by measuring also the oxygen content using the hydrogen reduction method. The points of Yazawa and Kameda must correspond to variable values of $P(SO_2)$ that are rather low but higher than for the slag–matte–SiO₂–metal equilibrium, which means that there is a disagreement between these data and the results of Chen et al.^[6] The lines calculated in the present study are based on the model parameters that were optimized in the lower-order systems. The model for the matte was adopted from earlier studies.^[18–25] In particular, the phase diagram in the Cu-Fe-S system shows a deviation of the matte composition towards excess metal at low $P(S_2)$ (see Shishin,^[21] Chapter 3.3). Hence, the sulfur content is expected to be lower and the iron content to be higher at metal saturation than at high $P(SO_2)$.

Figure 3 summarizes the composition of the liquid metallic copper for the slag–matte–SiO₂–metal equilibria. Iron in the liquid copper decreases with matte grade due to oxidation into the slag phase (Fig. 3a). Since the Fe-O pair interactions in the liquid metal are much stronger than the

Cu-O interactions, oxygen is present mostly in the Fe-O FNN pairs. Because of this, the oxygen content in the liquid diminishes when the iron content goes down until there is almost no iron left in the liquid copper phase and the equilibrium $P(O_2)$ rises sharply (Fig. 2a), allowing some Cu-O pairs to form, which results in the increasing oxygen content as wt.% Cu in the matte approaches 80 (Fig. 3b). The sulfur content remains fairly constant since $P(S_2)$ does not change much (Fig. 2b) and the Fe-S and Cu-S pair interactions are of comparable strength.

Tavera and Bedolla^[49] reported much higher oxygen and much lower sulfur content in the metal (Fig. 3b, 3c, diamonds). As was mentioned earlier in Sect. 3, the Gibbs phase rule was violated in their experimental setup, which resulted in non-equilibrium composition of copper. The oxygen partial pressure that was imposed on the system (Fig. 2a) was likely higher than the equilibrium values, which also lead to higher Fe³⁺ in the slag (Fig. 2g). The experimental data of Chen et al.^[6,7] and of Geveci and Rosenqvist^[36] are rather scattered, but they confirm the trends of the calculated lines and it is possible to see an increase in the solubility of sulfur in the metal with rising temperature.

Fig. 3 Composition of the liquid Cu-Fe alloy for the slag–matte–metal equilibria in the Cu-Fe-O-S-Si system at fixed temperature, total pressure of 1 atm. and tridymite (SiO₂) saturation. Symbols are experimental data^[6,7,36,49]; lines are calculated using the models of the present study. Different lines show the effect of temperature



3.3 Slag–Matte Equilibria: Effect of the Fe/SiO₂ Ratio in the Slag

Experimental indications that the Fe/SiO₂ ratio in the slag has an effect on the Cu and S solubility in the slag can be found in the works of Yazawa^[53] and of Takeda.^[40] It was demonstrated that increasing SiO₂ in the slag resulted in a drop of sulfur and copper in the slag. However, the former study was limited only to metal saturation conditions at 30 wt.% matte grade, and the latter was restricted to MgO-contaminated slags. Changes in the matte composition were not studied.

The recent studies of Hidayat et al.,^[8,9] employing a spinel–substrate technique, provide a dataset for the quantitative description of the effect of the Fe/SiO₂ ratio in the slag in the Cu-Fe-O-S-Si system (see Fig. 4). Studies of the matte/spinel equilibria in the SiO₂-free Cu-Fe-O-S system were also conducted by Hidayat et al.^[10,11] and are included in Fig. 4.

The minimum and maximum values of the Fe/SiO₂ ratio in the slag correspond to silica and spinel saturation, respectively (Fig. 4g). The composition of spinel in equilibrium with the slag is close to magnetite, Fe₃O₄. Hence, the slag has more Fe³⁺ in equilibrium with spinel than at silica saturation (Fig. 4f), which implies a higher equilibrium oxygen partial pressure (Fig. 4a). Accordingly, $P(S_2)$ is lower at the same $P(SO_2)$ (Fig. 4b). A corresponding small decrease in the sulfur content of the matte (Fig. 4e) is

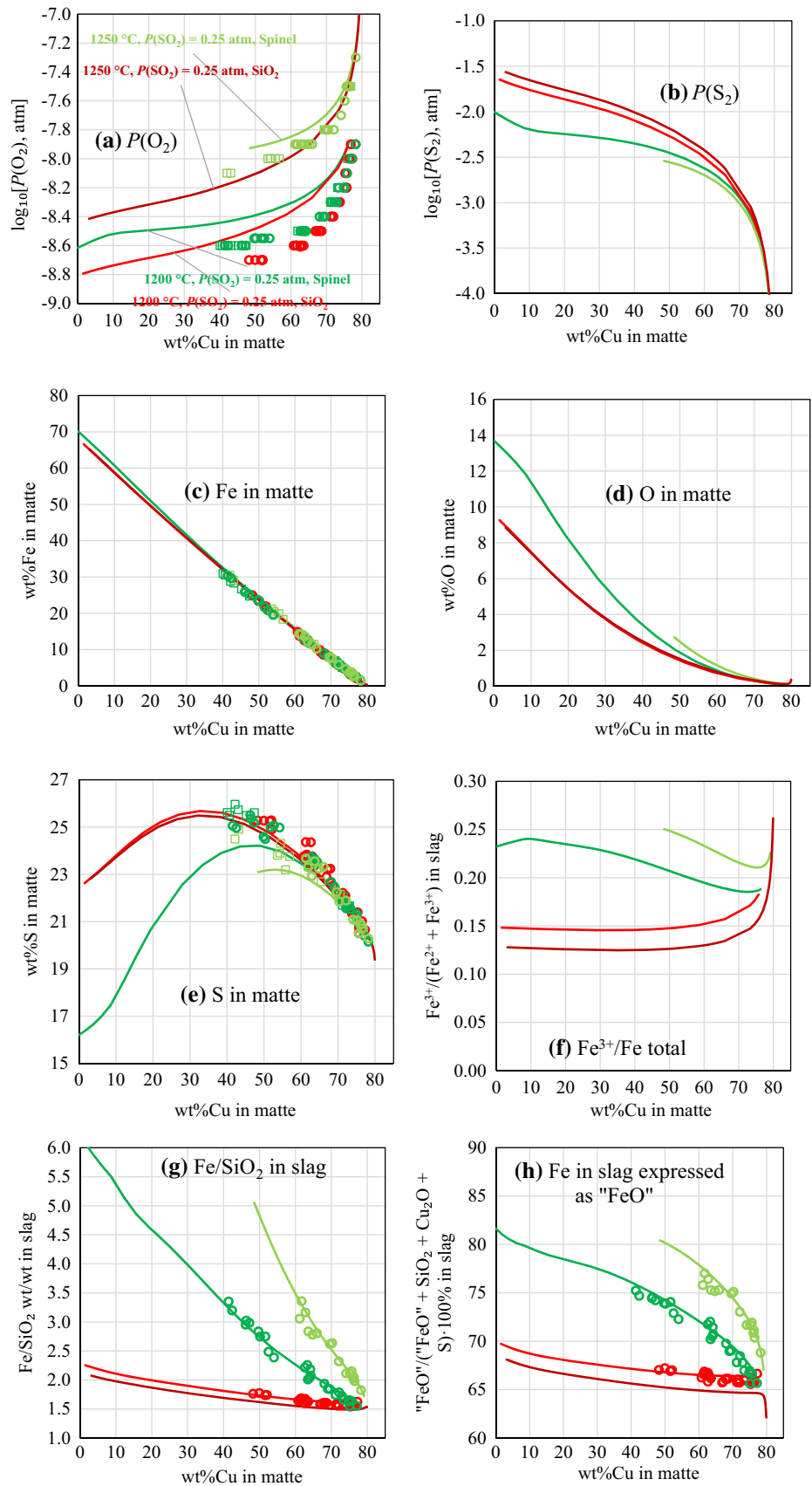
evident from the data of Hidayat et al.^[8,9] Qualitatively, the data of Kameda and Yazawa^[32] obtained at low $P(SO_2)$ in the flow of N₂ confirm the decrease in the S content and increase in the O content of the matte with increasing Fe/SiO₂ ratio. These data are not shown in Fig. 4.

As will be shown in Sect. 4, the exchange reaction among pure liquid oxides and sulfides, $FeO + 0.5SiS_2 = FeS + 0.5SiO_2$, is characterized by a very negative Gibbs energy, which results in strong FNN cation–anion short-range ordering, i.e. the Fe-S and Si-O pairs in the slag predominate at the expense of the Fe-O and Si-S pairs. Hence, the high Fe/SiO₂ ratio at spinel saturation is beneficial for the solubility of sulfur in the slag (Fig. 4i). This, in turn, increases the solubility of Cu in the slag as discussed earlier in Sect. 3.1. The balance of the increasing $P(O_2)$ and decreasing sulfur content accounts for the local minimum in the copper content at intermediate matte grades, which becomes more pronounced at spinel than at silica saturation due to the higher Fe/SiO₂ ratios in the slag (Fig. 4j). At matte grade approaching 80 wt.%, the slag reaches double SiO₂–spinel saturation (Fig. 4g) at 1200 °C, but not at 1250 °C.

3.4 Phase Equilibria in the Fe-O-S-Si System

The oxide and sulfide liquids are completely miscible in the Fe-O-S system.^[24] This oxysulfide liquid is propagated into the Fe-O-S-Si system, but a miscibility gap between the

Fig. 4 Slag–matte equilibria in the Cu–Fe–O–S–Si system at fixed temperature, total pressure of 1 atm., tridymite (SiO₂) or spinel saturation and fixed $P(\text{SO}_2)$. Symbols are experimental data,^[8,9,13] lines are calculated using the models of the present study. Experimental points^[10,11] for matte–spinel equilibria in the Cu–Fe–O–S system at fixed temperature, total pressure of 1 atm. and fixed $P(\text{SO}_2)$ are also shown



oxide- and sulfide-rich liquids appears and rapidly expands as the concentration of Si increases. The miscibility gap reported by Yazawa and Kameda^[54] at iron saturation is shown in Fig. 5. The composition of the slag and matte at double saturation with iron and SiO₂ was also studied by Takeda^[51] and Shimpo et al.^[48] (only the slag composition was reported in the latter study). The data on the slag–matte–SiO₂–Fe equilibrium at several temperatures are shown in Fig. 6. MacLean^[41] obtained similar results on the miscibility gap at higher $P(\text{SO}_2)$.

Some discrepancy between the experimental data is evident from Fig. 5 and 6. It should be noted that Yazawa and Kameda^[54] prepared their samples from stoichiometric FeS, FeO and SiO₂ and analyzed the quenched samples for Fe, S and SiO₂, assuming that the total amount of S is combined with iron as FeS and the remaining amount of iron is present as FeO. Hence, the reported slag and matte compositions are located exactly in the FeO–FeS–SiO₂ plane in Fig. 5, i.e. the presence of Fe₂O₃ in the oxide-rich liquid and the excess of metal in the sulfide-rich liquid was neglected. On the other hand, as can be seen from Fig. 6, Takeda^[51] reported substantial deviations from the FeO–FeS–SiO₂ plane for both slag and matte compositions based on the analysis of these liquids for Fe, S, O and SiO₂.

As mentioned earlier in Sect. 2, the slag and matte/metal phases are modeled in the present study as two separate solutions. This does not allow to reproduce the miscibility gap in the oxysulfide liquid shown in Fig. 5, because the calculations always give the slag + matte mixture instead of one oxysulfide liquid. However, the equilibrium of the slag and matte at SiO₂ saturation is reproduced within the uncertainty of the experimental data as can be seen from Fig. 5 and 6. The miscibility gap in the oxysulfide liquid rapidly expands as Cu, CaO, MgO, Al₂O₃ and other components are added to the system. Since the chemical systems of importance to pyrometallurgy are always far from the Fe–O–S subsystem, the inability of the slag and matte/metal models to describe the oxysulfide liquid is not important for practical applications. On the other hand, these models adequately reproduce the presence of Fe₂O₃ in the slag phase even in equilibrium with metal and the excess of metal or sulfur in the matte phase. Furthermore, the models for the slag and matte/metal explicitly account for the most important interactions in these phases, while remaining relatively simple. This greatly increases predictive ability of the models and makes it much easier to add new components to the thermodynamic database, using only limited available experimental data.

The model for the slag phase described in Sect. 2.1 can also be used for the matte if the deviations from the oxysulfide stoichiometry are neglected. This was done by Jo et al.,^[43] who also neglected the presence of Fe³⁺ in the slag/matte and used a separate solution for the liquid metal

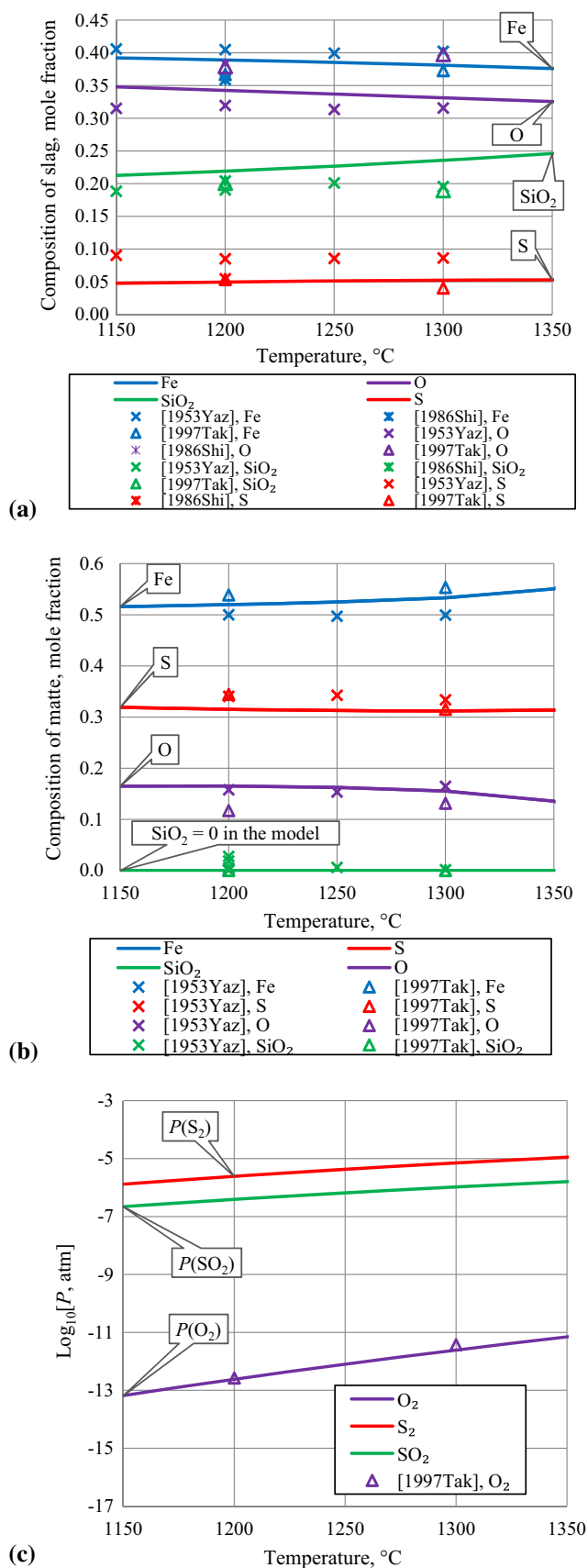


Fig. 6 Slag–matte–SiO₂–Fe equilibrium in the Fe–O–S–Si system as a function of temperature at total pressure of 1 atm. Experimental points^[48,51,54] and calculated lines

phase. The miscibility gap data of Yazawa and Kameda^[54] shown in Fig. 5 were well reproduced. However, this approach is not suitable for simulating pyrometallurgical production of copper because the experimental data for the Cu–Fe–O–S–Si system discussed above in Sect. 3.1–3.3 cannot be adequately described if the deviations of the matte composition from the oxysulfide stoichiometry are neglected.

The solubility of sulfur in slags is often described^[55] using the sulfide capacity, C_s . The definition of the sulfide capacity and the summary of experimental data for the Fe–O–S–Si system are shown in Fig. 7. These data are obtained by equilibration of the slags with a flow of gas, i.g. CO–CO₂–SO₂–Ar or H₂–CO₂–SO₂–N₂, which should define the partial pressures of both O₂ and S₂ in the system. The authors of the latest experimental study^[56] acknowledged the difficulties of attaining equilibrium between the slag and gas phases. They suggested that slower kinetics at low temperatures may have resulted in larger uncertainty of the data of Simeonov et al.,^[57] who reported much higher apparent temperature dependence of C_s than measured by Nzotta et al.^[56] In the present study, more weight is given to the data on the sulfur content of the slags in equilibrium with the matte in the Cu–Fe–O–S–Si system (see Fig. 1i, 2j), because equilibrating the condensed phases with the gas at relatively high fixed $P(\text{SO}_2)$ is believed to be easier than fixing two relatively low chemical potentials in the slag phase by equilibration with

the gas flow. The slag–matte equilibria can be extrapolated to zero matte grade and recalculated to sulfide capacity as shown in Fig. 7. The sulfide capacity obtained from the slag–matte equilibria seems to be somewhat inconsistent with C_s from the slag–gas equilibration experiments. The slag model cannot describe both sets of data simultaneously and gives systematically higher values of C_s compared to the slag–gas data.

4 Results and Discussion of Thermodynamic Modeling

4.1 Model Parameters of the Present Study

The model parameters for the matte, sulfur-free slag and solid phases were adopted from the previous works.^[18–28] Only sulfur-related model parameters for the slag phase were optimized in the present study. The numerical values are given in Table 2.

The Gibbs energies g_{FeS}° , $g_{\text{Fe}_2\text{S}_3}^\circ$, $g_{\text{SiS}_2}^\circ$ of pure components largely determine the sulfur content of the slag, while $g_{\text{Cu}_2\text{S}}^\circ$ has very strong effect on the copper content of the slag. $g_{\text{SiS}_2}^\circ$ was taken from Kang and Pelton.^[55] The entropy and heat capacity functions for pure liquid FeS, Fe₂S₃ and Cu₂S were obtained using the optimized properties of the liquid matte/metal solution at the corresponding compositions. The enthalpies of formation were optimized using the experimental data.

When the slag phase contains sulfur, FNN SRO can occur, the extent of which is related to the Gibbs energies of the reciprocal exchange reactions between pure liquid components shown in Table 3. Since these Gibbs energies are negative, the nearest-neighbor-pairs corresponding to components on the right side of the reactions predominate. For example, the Fe–O and Cu–S pairs in the slag predominate at the expense of the Fe–S and Cu–O pairs according to the first reaction in Table 3.

The positive parameter $g_{\text{Si}^{4+}\text{Fe}^{2+}/\text{O}^{2-}\text{O}^{2-}(\text{S}^{2-})}^{101}$ was necessary to adequately describe the effect of the Fe/SiO₂ ratio on the sulfur content in the slag (Fig. 4i), which also influenced the solubility of copper in the slag (Fig. 4j). The quantitative description of the local maximum and minimum on the Cu solubility curves required also positive parameters $\Delta g_{\text{Fe}^{2+}\text{Fe}^{2+}/\text{O}^{2-}\text{S}^{2-}}^\circ$ and $\Delta g_{\text{Cu}^{1+}\text{Cu}^{1+}/\text{O}^{2-}\text{S}^{2-}}^\circ$, as well as negative parameters $g_{\text{Fe}^{2+}\text{Cu}^{1+}/\text{S}^{2-}\text{S}^{2-}}^{10}$ and $g_{\text{Fe}^{3+}\text{Cu}^{1+}/\text{S}^{2-}\text{S}^{2-}}^{10}$.

The optimized model parameters provide a good agreement with the experimental data. Small systematic deviations of 0.1–0.25 in $\log_{10}[P(\text{O}_2), \text{atm.}]$ are observed for the $P(\text{O}_2)$ versus matte grade curves in Fig. 1(a), 2(a) and 4(a). As explained in Sect. 3.1, these curves are

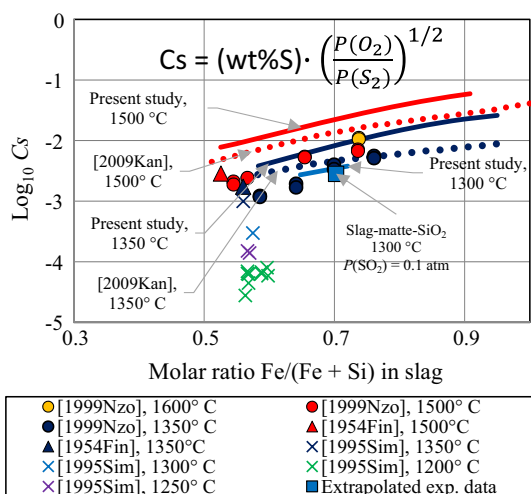


Fig. 7 Sulfide capacity of the slag in the Fe–O–S–Si system. Experimental points.^[12,47,51,56,57,69] Calculated lines correspond to Temperature/ $\log_{10}[P(\text{O}_2), \text{atm.}]/\log_{10}[P(\text{S}_2), \text{atm.}]$: 1300 °C/– 8.4/– 1.8, 1350 °C/– 7/– 3, 1500 °C/– 7/– 3. Dotted lines are calculated by the model of Kang and Pelton.^[55] Solid lines are calculated by the model of the present study

Table 2 Model parameters for the slag phase optimized in the present study

Parameter	Temperature range, K	Molar Gibbs energy $g(T)$, J mol ⁻¹	Coordination numbers
g_{FeS}^0	298.15–3000	$-123546.3 + 501.6241T - 80.49697\ln T + 391377.2T^{-1} - 7.0835 \cdot 10^{-3}T^2$	$Z_{\text{AB}/\text{XY}}^{\text{Fe}^{2+}} = Z_{\text{AB}/\text{XY}}^{\text{S}^{2-}} = Z_{\text{AB}/\text{XY}}^{\text{O}^{2-}} = 1.37744$
$g_{\text{Fe}_2\text{S}_3}^0$	298.15–1500	$-241834.0 + 1253.1420T - 203.37007\ln T + 1132326.3T^{-1} - 1.0763 \cdot 10^{-2}T^2$	$Z_{\text{AB}/\text{XY}}^{\text{Fe}^{3+}} = 2.06617$
$g_{\text{SiS}_2}^0$	1500–3000	$-263251.3 + 1481.6272T - 234.79927\ln T$	$Z_{\text{AB}/\text{XY}}^{\text{Si}^{4+}} = 2.75489$
$g_{\text{Cu}_2\text{S}}^0$	298.15–3000	$-283896.9 + 621.8719T - 100.00007\ln T$	$Z_{\text{AB}/\text{XY}}^{\text{Cu}^{1+}} = 0.68872$
	298.15–1500	$-71017.7 + 375.9011T - 75.24437\ln T + 121819.3T^{-1} - 1.0213 \cdot 10^{-2}T^2$	where A and B are Fe ²⁺ , Fe ³⁺ , Si ⁴⁺ , Cu ¹⁺
	1500–3000	$-84985.3 + 520.097T - 95.10907\ln T - 3.2500 \cdot 10^{-3}T^2$	X and Y are O ²⁻ , S ²⁻
$\Delta g_{\text{Fe}^{2+}\text{Fe}^{3+}/\text{O}^{2-}\text{S}^{2-}}^0$		$42915.3 - 37.6560T$	except for the following coordination numbers:
$g_{\text{Si}^{4+}\text{Fe}^{2+}/\text{O}^{2-}\text{S}^{2-}}^{101}$		196648.0	$Z_{\text{AB}/\text{XY}}^{\text{Fe}^{3+}} = Z_{\text{Cu}^{1+}\text{Fe}^{2+}/\text{O}^{2-}\text{O}^{2-}} = Z_{\text{Cu}^{1+}\text{Si}^{4+}/\text{O}^{2-}\text{O}^{2-}} = 1.37744375$
$\Delta g_{\text{Cu}^{1+}\text{Cu}^{1+}/\text{O}^{2-}\text{S}^{2-}}^0$		29288.0	$\zeta_{\text{Fe}^{2+}\text{S}^{2-}} = \zeta_{\text{Fe}^{2+}\text{O}^{2-}} = 1.377$
$g_{\text{Fe}^{2+}\text{Cu}^{1+}/\text{S}^{2-}\text{S}^{2-}}^{10}$		$110708.6 - 83.6800T$	$\zeta_{\text{Fe}^{3+}\text{S}^{2-}} = \zeta_{\text{Fe}^{3+}\text{O}^{2-}} = 1.653$
$g_{\text{Fe}^{3+}\text{Cu}^{1+}/\text{S}^{2-}\text{S}^{2-}}^{10}$		$102340.6 - 83.6800T$	$\zeta_{\text{Si}^{4+}\text{S}^{2-}} = \zeta_{\text{Si}^{4+}\text{O}^{2-}} = 1.837$
			$\zeta_{\text{Cu}^{1+}\text{S}^{2-}} = \zeta_{\text{Cu}^{1+}\text{O}^{2-}} = 0.918$

Parameters notations are available in Pelton et al.,^[44] Eq 45. $\zeta_{A,X}$, the modified ratio of FNN–SNN coordination numbers is defined in Eq 2.22 by Lambotte^[30]

Table 3 Standard Gibbs energies of reciprocal exchange reactions at 1200 °C, governing the first-nearest-neighbor short-range ordering

Reciprocal reaction	$\Delta G_{AB/O^2-S^2-}^{o,exchange}$, kJ mol ⁻¹
$Cu_2O + FeS = Cu_2S + FeO$	- 105
$3FeO + Fe_2S_3 = 3FeS + Fe_2O_3$	- 46
$3Cu_2O + Fe_2S_3 = 3Cu_2S + Fe_2O_3$	- 361
$Cu_2O + 0.5SiS_2 = Cu_2S + 0.5SiO_2$	- 257
$FeO + 0.5SiS_2 = FeS + 0.5SiO_2$	- 152
$Fe_2O_3 + 1.5SiS_2 = Fe_2S_3 + 1.5SiO_2$	- 410

practically independent of the model parameters of the presents study and predicted based on the assessments of the low-order systems.^[18–28] They are supported by the data of Takeda.^[40,51]

In addition to the dataset for the Cu-Fe-O-S-Si system discussed above, experimental studies of the slag–matte equilibria in the Ca-Cu-Fe-O-S system by Park et al.,^[58] Acuna and Yazawa^[59] and Roghani et al.^[60] were taken into account. The calcium ferrite slags dissolve significantly more Cu and S than the fayalite slags, which was successfully reproduced by the model. The effect of CaO, MgO and Al₂O₃ on slag–matte equilibria in the Cu-Fe-O-S-Si system will be reported elsewhere.

4.2 A Note on the “Oxidic” and “Sulfidic” Solubility of Cu in the Slag

In the works of Sehnalek and Imris,^[61] as well as Nagamori,^[37] it was suggested to represent the total dissolved copper in the slag as a sum of “oxidic” and “sulfidic” components. This terminology was adopted by Yazawa^[53] and is widely used in non-ferrous metallurgy. Overall, the “oxidic/sulfidic” concept was introduced to describe the maximum on the Cu solubility in slag versus Cu in matte (see Fig. 1j) and other relationships among $P(O_2)$, $P(S_2)$ and the composition of slag and matte observed experimentally.^[61–63] Similar “oxidic/sulfidic” concepts were applied by some researchers to explain the solubility of nickel^[64] and lead^[39] in the slag. As a consequence, thermodynamic models were developed later, where Cu₂O and Cu₂S were taken as the components of the slag solution, for instance in the study of Tan.^[65] These components were treated as randomly mixing molecular associates, which is not consistent with the real nature of liquid slags.

More recently, superior slag models were developed. The Modified Quasichemical Formalism in the Quadruplet Approximation (MQMQA) that reflects the ionic nature of slags is used in the present study. It explains the interrelation between the solubility of copper and sulfur in the

slag as the result of first-nearest-neighbor (cation–anion) short-range ordering, which is caused by the strong inter-ionic interactions. Furthermore, this model explicitly takes into account the second-nearest-neighbor short-range ordering of basic and acidic cations. Compared to the associate models, the MQMQA gives more accurate description of the slag properties and has better predictive ability. This was discussed in more detail by Pelton.^[66]

4.3 Applications of the Thermodynamic Database

Selective distribution of elements among the slag, matte, metal and gas phases is the basis for pyrometallurgical production of copper from sulfide concentrates. Understanding of the thermochemistry is necessary for metallurgists to predict the trends in a multidimensional space of process parameters and conditions. Examples of the process conditions and variables are temperature, oxygen enrichment, fluxing, composition of the concentrate, strategies for internal streams recycling, etc. The industry faces a general tendency for increasing amounts of impurities in concentrates, stricter environmental regulations, and the need to utilize secondary materials. In response to the growing complexity, computer-based numerical tools are created for prediction of partitioning of major and minor elements among phases and for computation of liquidus and heat balance. These tools are used for the gradual transition from the back-feed control to forward-feed control of furnace operation, as well as for global economic optimization of the process flowsheet. A proper simulation of a chemical reactor must take into account both thermodynamics and kinetics. However, a firm foundation in chemical thermodynamics of the basic systems is an essential prerequisite for introducing kinetic factors. Cu-Fe-O-S-Si is the basic chemical system for copper smelting. Examples of the application of thermodynamic calculations for the simulation of Peirce-Smith converter and Isasmelt furnace can be found elsewhere.^[67,68]

The developed thermodynamic database makes it possible to represent the slag liquidus in a form that is more familiar to furnace operators. For example, Fig. 8 shows the tridymite and spinel liquidus lines as a function of the Fe/SiO₂ ratio in the slag. Clearly, the slag equilibrated with the matte of certain matte grade at fixed $P(SO_2)$ will remain fully liquid in the region between the tridymite liquidus line on the left and spinel liquidus on the right. As can be seen from Fig. 8, matte grade and $P(SO_2)$ have a large effect on the spinel liquidus. It should be noted that the presence of Al₂O₃, CaO and MgO will normally shift the liquidus lines to the left and may introduce other changes, which will be discussed in a future publication.

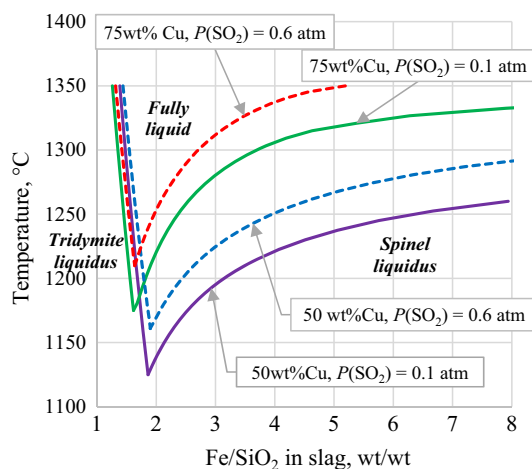


Fig. 8 Liquidus in the Cu-Fe-O-S-Si system for the fayalite slag equilibrated with the matte. Lines are calculated using the optimized model parameters of the present study. Labels show fixed wt.% Cu in the matte and $P(\text{SO}_2)$

5 Conclusion

The existing experimental studies of the slag–matte and slag–matte–metal equilibria in the Cu-Fe-O-S-Si system have been summarized and critically assessed. In particular, the recent experimental results have clarified the relationships among matte grade, temperature, $P(\text{SO}_2)$, Fe/SiO₂ in the slag, chemical solubility of Cu and S in the slag, O and S contents in the matte and metal, $P(\text{O}_2)$ and $P(\text{S}_2)$. Thermodynamic models have been developed for the slag and matte/metal phases within the framework of the Modified Quasichemical Formalism, which made it possible to describe these relationships within the uncertainty of the experimental data. Large deviations from ideal mixing can occur in the slag due to the strong first-nearest-neighbor (cation–anion) interactions. The resulting short-range ordering elucidates the interrelationship between the copper and sulfur solubility in the slag. The present article is part of a larger project aimed at the developing of a fully consistent thermodynamic database for the Al-Ca-Cu-Fe-Mg-O-Pb-S-Si-Zn-(As, Bi, Sb, Ag, Au) chemical system.

Acknowledgments The authors would like to thank Australian Research Council, linkage project LP140100480 “Creating sustainable copper supplies by using innovative high temperature chemical processing of highly complex impure ores and recycled materials”. We appreciate the financial and technical support by the consortium of copper producers: Umicore NV, Aurubis AG, Kazzinc Ltd (Glencore), Outotec Oy, Complejo Metalúrgico Altonorte, Atlantic Copper, BHP Billiton Olympic Dam Corporation, PASAR (Glencore), Anglo American Platinum, Kennecott (Rio Tinto).

References

1. S.A. Degterov and A.D. Pelton, A Thermodynamic Database for Copper Smelting and Converting, *Metall. Mater. Trans. B*, 1999, **30B**, p 661-669
2. E. Jak, P. Hayes, C.W. Bale, and S.A. Dechterov, Application of FactSage Thermodynamic Modeling of Recycled Slags (Al₂O₃-CaO-FeO-Fe₂O₃-SiO₂-PbO-ZnO) in the Treatment of Wastes from End-of-Life-Vehicles, *Int. J. Mater. Res.*, 2007, **98**, p 872-878
3. E. Jak, S.A. Dechterov, B. Zhao, A.D. Pelton, and P.C. Hayes, Coupled Experimental and Thermodynamic Modelling Studies for Metallurgical Smelting and Coal Combustion Slag Systems, *Metall. Mater. Trans. B*, 2000, **31B**, p 621-630
4. E. Jak, S.A. Dechterov, P.C. Hayes, and A.D. Pelton, in *Thermodynamic Modelling of the System PbO-ZnO-FeO-Fe₂O₃-CaO-SiO₂ for Zinc/Lead Smelting*. Proceedings of 5th International Conference on Molten Slags, Fluxes and Salts, Iron and Steel Society, AIME, Sydney, 1997, pp. 621–628
5. C.W. Bale, E. Belisle, P. Chartrand, S.A. Dechterov, G. Eriksson, K. Hack, I.-H. Jung, Y.-B. Kang, J. Melancon, A.D. Pelton, C. Robelin, and S. Petersen, FactSage Thermochemical Software and Databases—Recent Developments, *CALPHAD*, 2009, **33**, p 295-311
6. J. Chen, P.C. Hayes, and E. Jak, in *Experimental Investigation of Slag/Matte/Metal/Tridymite Equilibrium in the Cu-Fe-O-S-Si System at T = 1200 °C: Development of Technique and Results*. Internal Report University of Queensland, 2017
7. J. Chen, P.C. Hayes, and E. Jak, in *Experimental Investigation of Slag/Matte/Metal/Tridymite Equilibrium in the Cu-Fe-O-S-Si System at T = 1250 and 1300 °C*. Internal Report University of Queensland, 2017
8. T. Hidayat, A. Fallah-Mehrjardi, P.C. Hayes, and E. Jak, Experimental Investigation of Gas/Slag/Matte/Spinel Equilibria in the Cu-Fe-O-S-Si System at T = 1250 °C and $P(\text{SO}_2) = 0.25$ atm, *Metall. Mater. Trans. B*, 2018, submitted
9. T. Hidayat, A. Fallah-Mehrjardi, P.C. Hayes, and E. Jak, Experimental Investigation of Gas/Slag/Matte/Spinel Equilibria in the Cu-Fe-O-S-Si System at 1473 K (1200 °C) and $P(\text{SO}_2) = 0.25$ atm, *Metall. Mater. Trans. B*, 2018, **49**, p 1750-1765
10. T. Hidayat, A. Fallah-Mehrjardi, P.C. Hayes, and E. Jak, Experimental Investigation of Gas/Matte/Spinel Equilibria in the Cu-Fe-O-S System at T = 1200 °C and $P(\text{SO}_2) = 0.25$ atm, *Metall. Mater. Trans. B*, 2018, submitted
11. T. Hidayat, P.C. Hayes, and E. Jak, Experimental Investigation of Gas/Matte/Spinel Equilibria in the Cu-Fe-O-S System at T = 1250 °C and $P(\text{SO}_2) = 0.25$ atm, *Metall. Mater. Trans. B*, 2018, submitted
12. A. Fallah-Mehrjardi, T. Hidayat, P.C. Hayes, and E. Jak, Experimental Investigation of Gas/Slag/Matte/Tridymite Equilibria in the Cu-Fe-O-S-Si system in Controlled Gas Atmosphere: Experimental Results at T = 1523 K (1250 °C) and $P(\text{SO}_2) = 0.25$ atm, *Metall. Mater. Trans. B*, 2018, **49**, p 1732-1739
13. A. Fallah-Mehrjardi, T. Hidayat, P.C. Hayes, and E. Jak, Experimental Investigation of Gas/Slag/Matte/Tridymite Equilibria in the Cu-Fe-O-S-Si System in Controlled Gas Atmospheres: Experimental Results at T = 1473 K [1200 °C] and $P(\text{SO}_2) = 0.25$ atm, *Metall. Mater. Trans. B*, 2017, **48**, p 3017-3026
14. A. Fallah-Mehrjardi, T. Hidayat, P.C. Hayes, and E. Jak, Experimental Investigation of Gas/Slag/Matte/Tridymite Equilibria in the Cu-Fe-O-S-Si system in Controlled Gas Atmo-

- spheres: Development of Technique, *Metall. Mater. Trans. B*, 2017, **48**, p 3002-3016
15. A. Fallah-Mehrjardi, P.C. Hayes, and E. Jak, Experimental Investigation of Gas/Slag/Matte/Tridymite Equilibria in the Cu-Fe-O-S-Si system in Controlled Gas Atmospheres: Experimental Results at $T = 1473$ K [1200 °C] and $P(\text{SO}_2) = 0.1, 0.25, 0.6$ atm, *Metall. Mater. Trans. B*, 2018, submitted
 16. A. Fallah-Mehrjardi, P.C. Hayes, and E. Jak, Experimental Investigation of Gas/Slag/Matte/Tridymite Equilibria in the Cu-Fe-O-S-Si-Mg System in Controlled Gas Atmospheres: Experimental Results at $T = 1473$ K [1200 °C] and $P(\text{SO}_2) = 0.25$ atm, *Metall. Mater. Trans. B*, 2018, submitted
 17. E. Jak, T. Hidayat, D. Shishin, A.F. Mehrjardi, J. Chen, and P. Hayes, in *Integrated Experimental Phase Equilibria and Thermodynamic Modelling Studies for Copper Pyrometallurgy*. 9th International Copper Conference, Kobe, Japan, 2016
 18. T. Hidayat, D. Shishin, E. Jak, and S. Decterov, Thermodynamic Reevaluation of the Fe-O System, *CALPHAD*, 2015, **48**, p 131-144
 19. P. Waldner and A.D. Pelton, Thermodynamic Modeling of the Fe-S System, *J. Phase Equilib. Diffus.*, 2005, **26**, p 23-28
 20. P. Waldner and A.D. Pelton, in *Thermodynamic Modeling of the Cu-Fe-S System*. Internal Report, Ecole Polytechnique de Montreal (Montreal, QC, Canada), 2006
 21. D. Shishin, in *Development of a Thermodynamic Database for Copper Smelting and Converting*, Ph. D. Thesis, École Polytechnique de Montréal, 2013
 22. D. Shishin and S.A. Decterov, Critical Assessment and Thermodynamic Modeling of Cu-O and Cu-O-S Systems, *CALPHAD*, 2012, **38**, p 59-70
 23. D. Shishin, T. Hidayat, E. Jak, and S. Decterov, Critical Assessment and Thermodynamic Modeling of Cu-Fe-O System, *CALPHAD*, 2013, **41**, p 160-179
 24. D. Shishin, E. Jak, and S.A. Decterov, Critical Assessment and Thermodynamic Modeling of the Fe-O-S System, *J. Phase Equilib. Diffus.*, 2015, **36**, p 224-240
 25. D. Shishin, E. Jak, and S.A. Decterov, Thermodynamic Assessment and Database for the Cu-Fe-O-S System, *CALPHAD*, 2015, **50**, p 144-160
 26. T. Hidayat and E. Jak, Thermodynamic Modeling of the “Cu₂O”-SiO₂, “Cu₂O”-CaO, and “Cu₂O”-CaO-SiO₂ Systems in Equilibrium with Metallic Copper, *Int. J. Mater. Res.*, 2014, **105**, p 249-257
 27. T. Hidayat, D. Shishin, S.A. Decterov, and E. Jak, Experimental Study and Thermodynamic Re-evaluation of the FeO-Fe₂O₃-SiO₂ System, *J. Phase Equilib. Diffus.*, 2017, **38**, p 477-492
 28. T. Hidayat, D. Shishin, S. Decterov, and E. Jak, Critical Assessment and Thermodynamic Modeling of the Cu-Fe-O-Si System, *CALPHAD*, 2017, **58**, p 101-114
 29. C.W. Bale, E. Belisle, P. Chartrand, S.A. Decterov, G. Eriksson, A.E. Gheribi, K. Hack, I.H. Jung, Y.B. Kang, J. Melancon, A.D. Pelton, S. Petersen, C. Robelin, J. Sangster, P. Spencer, and M.A. Van Ende, FactSage Thermochemical Software and Databases, 2010-2016, *CALPHAD*, 2016, **54**, p 35-53
 30. G. Lambotte, in *Approche Thermodynamique de la Corrosion des Réfractaires Aluminosiliceux par le Bain Cryolithique : Modélisation Thermodynamique du Système Quaternaire Réciproque AlF₃-NaF-SiF₄-Al₂O₃-Na₂O-SiO₂*. Ph. D. Thesis, École Polytechnique de Montréal, 2012
 31. A. Yazawa and M. Kameda, Fundamental Studies on Copper Smelting. IV. Solubility of FeO in Copper Matte from SiO₂-saturated FeO-SiO₂ Slag, *Technol. Rep. Tohoku Univ.*, 1955, **19**, p 251-261
 32. M. Kameda and A. Yazawa, in *The Oxygen Content of Copper Mattes*, ed. by G.R.S. Pierre. Proceedings of Physical Chemistry of Process Metallurgy, Part 2, TMS Conference. Proceedings of Interscience, NY, 1961, pp. 963–988
 33. N. Korakas, *Etude Thermodynamique de l'équilibre Entre Scories Ferro-siliceuses et Mattes de Cuivre. Application aux Problèmes Posés par la Formation de Magnetite Lors du Traitement des Minerais Sulfurés de Cuivre*, Ph. D. Thesis, Université de Liège, 1964
 34. U. Kuxmann and F.Y. Bor, Studies on the Solubility of Oxygen in Copper Mattes under Ferric Oxide Slags Saturated with Silica, *Erzmetall*, 1965, **18**, p 441-450
 35. F.Y. Bor and P. Tarassoff, Solubility of Oxygen in Copper Mattes, *Can. Metall. Q.*, 1971, **10**, p 267-271
 36. A. Geveci and T. Rosenqvist, Equilibrium Relations between Liquid Copper, Iron-Copper Matte, and Iron Silicate Slag at 1250° , *Trans. Inst. Min. Metall.*, 1973, **82**, p C193-C201
 37. M. Nagamori, Metal Loss to Slag: Part I. Sulfidic and Oxidic Dissolution of Copper in Fayalite Slag from Low Grade Matte, *Metall. Trans. B*, 1974, **5B**, p 531-538
 38. F.J. Tavera and W.G. Davenport, Equilibrations of Copper Matte and Fayalite Slag under Controlled Partial Pressures of Sulfur Dioxide, *Metall. Trans. B*, 1979, **10B**, p 237-241
 39. G.H. Kairua, K. Watanabe, and A. Yazawa, The Behavior of Lead in Silica-Saturated Copper Smelting Systems, *Can. Metall. Q.*, 1980, **19**, p 191-200
 40. Y. Takeda, in *Copper Solubility in Matte Smelting Slag*. Proceedings of International Conference on Molten Slags, Fluxes Salts '97, 5th, Iron and Steel Society Warrendale, PA, 1997, pp. 329–339
 41. W.H. MacLean, Liquid Phase Relations in the FeS-FeO-Fe₃O₄-SiO₂ System, and Their Application in Geology, *Econ. Geol.*, 1969, **64**, p 865-884
 42. D. Dilner and M. Selleby, Thermodynamic Description of the Fe-Ca-O-S System, *CALPHAD*, 2017, **57**, p 118-125
 43. Y. Jo, H.-G. Lee, and Y.-B. Kang, Thermodynamics of the MnO-FeO-MnS-FeS-SiO₂ System at SiO₂ Saturation Under Reducing Condition: Immiscibility in the Liquid Phase, *ISIJ Int.*, 2013, **53**, p 751-760
 44. A.D. Pelton, P. Chartrand, and G. Eriksson, The Modified Quasichemical Model IV—Two Sublattice Quadruplet Approximation, *Metall. Mater. Trans. A*, 2001, **32**, p 1409-1415
 45. R. Piao, H.-G. Lee, and Y.-B. Kang, Experimental Investigation of Phase Equilibria and Thermodynamic Modeling of the CaO-Al₂O₃-CaS and the CaO-SiO₂-CaS Oxysulfide Systems, *Acta Mater.*, 2013, **61**, p 683-696
 46. H. Jalkanen, Copper and Sulfur Solubilities in Silica-Saturated Iron Silicate Slags from Copper Mattes, *Scand. J. Metall.*, 1981, **10**, p 177-184
 47. A. Yazawa, S. Nakazawa, Y. in *Takeda, Distribution Behavior of Various Elements in Copper Smelting Systems*, ed by H.Y. Sohn, D.B. George, A.D. Zunkel. Proceedings of International Sulfide Smelting Symposium on Extr. Process Metall. Meet. Metall. Soc. Advance Sulfide Smelting, AIME, 1983, pp. 99–117
 48. R. Shimpō, S. Goto, O. Ogawa, and I. Asakura, A Study on the Equilibrium Between Copper Matte and Slag, *Can. Metall. Q.*, 1986, **25**, p 113-121
 49. F.J. Tavera and E. Bedolla, Distribution of Copper, Sulfur, Oxygen and Minor Elements Between Silica-Saturated Slag, Matte and Copper—Experimental Measurements, *Int. J. Miner. Process.*, 1990, **29**, p 289-309
 50. H. Li and W.J. Rankin, Thermodynamics and Phase Relations of the Fe-O-S-SiO₂(sat) System at 1200 °C and the Effect of Copper, *Metall. Trans. B*, 1994, **25B**, p 79-89
 51. Y. Takeda, in *Oxygen Potential Measurement of Iron Silicate Slag-Copper-Matte System*. Proceedings of International Conference on Molten Slags, Fluxes Salts '97, 5th, Iron and Steel Society Warrendale, PA, 1997, pp. 735–743
 52. J.M. Font, G. Roghani, M. Hino, and K. Itagaki, Solubility of Copper or Nickel in Iron-Silicate Base Slag Equilibrated with

- Cu₂S-FeS or Ni₃S₂-FeS Matte Under High Partial Pressures of SO₂, *Metall. Rev. MMII*, 1998, **15**, p 75-86
53. A. Yazawa, Thermodynamic Considerations of Copper Smelting, *Can. Metall. Q.*, 1974, **13**, p 443-453
54. A. Yazawa and M. Kameda, Fundamental Studies on Copper Smelting. I. Partial Liquidus Diagram for FeS-FeO-SiO₂ System, *Technol. Rep. Tohoku Univ.*, 1953, **18**, p 40-58
55. Y.-B. Kang and A. Pelton, Thermodynamic Model and Database for Sulfides Dissolved in Molten Oxide Slags, *Metall. Mater. Trans. B*, 2009, **40**, p 979-994
56. M.M. Nzotta, D. Sichen, and S. Seetharaman, Sulfide Capacities of FeO-SiO₂, CaO-FeO, and FeO-MnO Slags, *ISIJ Int.*, 1999, **39**, p 657-663
57. S.R. Simeonov, R. Sridhar, and J.M. Toguri, Sulfide Capacities of Fayalite-Base Slags, *Metall. Trans. B*, 1995, **26B**, p 325-334
58. M.G. Park, Y. Takeda, and A. Yazawa, Equilibrium Relations Between Liquid Copper, Matte and Calcium Ferrite Slag at 1250 °C, *Tohoku Daigaku Senko Seiren Kenkyusho Iho*, 1983, **39**, p 115-122
59. C. Acuna and A. Yazawa, Mutual Dissolution Between Matte and Ferrite Slags, *Trans. Jpn. Inst. Met.*, 1986, **27**, p 881-889
60. G. Roghani, M. Hino, and K. Itagaki, Phase Equilibrium Between Calcium Ferrite Slag and Copper Matte at 1523 K Under High Partial Pressures of SO₂, *Mater. Trans. JIM*, 1996, **37**, p 1431-1437
61. F. Sehnalek and I. Imris, in *Slags from Continuous Copper Production*, ed. by M.J. Jones. Proceedings of International Symposium on Institution of Mining and Metallurgy, Advances in Extractive Metallurgy and Refining, London, England, 1972, pp. 39–62
62. P. Spira and N. Themelis, Solubility of Copper in Slags, *J. Met.*, 1969, **21**, p 35-42
63. E.-B. Johansen, T. Rosenqvist, and P.T. Torgersen, Thermodynamics of Continuous Copper Smelting, *J. Met.*, 1970, **22**, p 39-47
64. J.M. Font, Y. Takeda, and K. Itagaki, Phase Equilibrium Between Iron-Silicate Base Slag and Nickel-Iron Matte at 1573 K Under High Partial Pressures of SO₂, *Mater. Trans.*, 1998, **39**, p 652-657
65. P. Tan, in *CuModel—A Thermodynamic Model and Computer Program of Copper Smelting and Converting Processes and Its Industrial Applications*, ed. by M.E. Schlesinger. EPD Congress 2004, Proceedings of Sessions and Symposia held during the TMS Annual Meeting, Charlotte, NC, United States, Mar 14–18, 2004, Minerals, Metals and Materials Society, Warrendale, PA, 2004, pp. 411–422
66. A.D. Pelton, Thermodynamic Models and Databases for Slags, Fluxes and Salts, *Trans. Inst. Min. Metall. Sect. C*, 2005, **114**, p 172-180
67. D. Shishin, T. Hidayat, S. Decterov, and E. Jak, in *Thermodynamic Modelling of Liquid Slag-Matte-Metal Equilibria Applied to the Simulation of the Peirce-Smith Converter*. Proceedings of 10th International Conference on Molten Slags, Fluxes and Salts, Seattle, Seattle, USA, 2016
68. D. Shishin, T. Hidayat, E. Jak, S. Decterov, and G.V. Belov, Thermodynamic Database for Pyrometallurgical Copper Extraction, in *Proceedings of Copper'2016*, Kobe, Japan, 2016, p. 12
69. C.J.B. Fincham and F.D. Richardson, The Behaviour of Sulphur in Silicate and Aluminate Melts, *Proc. R. Soc. (Lond.)*, 1954, **223**, p 40-62
70. G. Eriksson and A.D. Pelton, Critical Evaluation and Optimization of the Thermodynamic Properties and Phase Diagrams of the CaO-Al₂O₃, Al₂O₃-SiO₂, and CaO-Al₂O₃-SiO₂ Systems, *Metall. Trans.*, 1993, **24**, p 807-816